2008

Tissue equivalence correction in silicon microdosimetry for protons characteristic of the LEO Space Environment

Susanna Guatelli
University of Wollongong, susanna@uow.edu.au

Mark I. Reinhard
Australian Nuclear Science and Technology Organisation, Lucas Heights, Sydney

B Mascialino
Dept Medical Epidemiology and Biostatistics, Karol, barbara.mascialino@ki.se

Dale A. Prokopovich
Australian Nuclear Science and Technology Organisation (ANSTO), dap11@uow.edu.au

A S. Dzurak
University of New South Wales

See next page for additional authors

Tissue equivalence correction in silicon microdosimetry for protons characteristic of the LEO space environment

S. Guatelli, *Member, IEEE,* M. I. Reinhard, *Member, IEEE,* B. Mascialino, D. A. Prokopovich, *Student Member, IEEE,* A. S. Dzurak, M. Zaider and A. B. Rosenfeld, *Senior Member, IEEE*

***Abstract*— The tissue equivalence of solid state silicon detectors in proton radiation fields was determined to improve the radiation protection applications of silicon detectors in aviation and space missions. The study was performed by means of Geant4 simulations. Results are presented showing that a simple geometrical scaling factor (~0.56) of linear dimensions is adequate to convert experimentally obtained microdosimetric energy deposition spectra in silicon to equivalent microdosimetric energy deposition spectra in water.**

***Index Terms*— Microdosimetry, Geant4, silicon detector, tissue equivalence.**

I. Introduction

Silicon On Insulator (SOI) microdosimeters have been under investigation for the past ten years as a possible alternative to tissue equivalent gas counters for microdosimetric measurements in medical physics and radiation protection [1, 2].

The advantages of microdosimeters based on solid state silicon are true microdosimetric sized sensitive volumes, low voltage operation and the elimination of the need for a tissue equivalent gas. The potentially compact size of such an instrument also lends to the possibility of use for personal dosimetry.

Applications of the technology include radiation protection for personnel in space and at nuclear facilities [3], radiation effects on microelectronics in space missions and aviation, dosimetry in medical physics [4, 5] and radiobiological research [6].

In particular SOI microdosimetric technology is being explored as a possible radiation monitoring system to adopt in spacecrafts to warn the crew of possible harmful Solar Particle Events (SPE) in real time [3].

A crucial issue in the eventual adoption of SOI microdosimeters is how to convert silicon based microdosimetric spectra to tissue equivalent material microdosimetric spectra.

Bradley and co-authors addressed the issue of tissue equivalence of silicon based microdosimetric measurements in the special case of Boron Neutron Capture Therapy (BNCT) radiation fields [7]. The tissue equivalence of a first generation silicon microdosimeter, based on a parallelepiped (RPP) silicon detector, was investigated. Comparisons of the range-energy relationships for ion products, generated by the interactions of neutrons with tissue and silicon were carried out.

In this paper the tissue equivalence of silicon is studied in the context of a second generation microdosimeter based on a cylindrical design of the silicon sensitive detector [8]. The applications of interest are astronaut radiation protection in space in the presence of protons from SPE, and dosimetry for protontherapy.

The study was performed by means of Geant4 simulations. Geant4 is a Monte Carlo toolkit for the simulation of the passage of particles through matter and the associated depositions of energy [9, 10].

In this study Geant4 is employed to simulate the microdosimetric spectra in micron-sized detectors exposed to the radiation environment of interest. A Geant4 capability for microdosimetry has been the subject of study in recent years and its accuracy in reproducing physical results with respect to experimental measurements is still a subject of ongoing investigation. Previous work has demonstrated good

Manuscript received July 11, 2008.

S. Guatelli is with the Australian Nuclear Science and Technology Organization (ANSTO), New Illawarra Road, Lucas Heights, NSW 2234, Australia (phone: +61-2-9717-7236; fax: +61-2-9717-9265; e-mail: susanna.guatelli@ ansto.gov.au).

M. I. Reinhard is with the Australian Nuclear Science and Technology Organization (ANSTO), New Illawarra Road, Lucas Heights, NSW 2234, Australia (e-mail: mark.reinhard@ansto.gov.au).

B. Mascialino is with the Department of Medical Epidemiology and Biostatistics, Karolinska Institutet, Nobels Väg 12 A, 17120 Stockholm Sweden (e-mail: barbara.mascialino@ki.se).

D. A. Prokopovich is with the Australian Nuclear Science and Technology Organization (ANSTO), New Illawarra Road, Lucas Heights, NSW 2234, Australia (e-mail: dale.prokopovich@ansto.gov.au).

A. S. Dzurak is with the School of Electrical Engineering & Telecommunications, University of New South Wales, Sydney, NSW 2052, Australia (e-mail: a.dzurak@unsw.edu.au).

M. Zaider is with the Department of Medical Physics, Memorial Sloan-Kettering Cancer Center, 1275 York Ave, New York, NY New York 10021, USA (e-mail: zaiderm@mskcc.org).

A. B. Rosenfeld is with the Centre for Medical Radiation Physics, University of Wollongong, Wollongong, NSW 2087, Australia, (e-mail: Anatoly@uow.edu.au).

agreement between Geant4 simulations and experimental data in the context of microdosimetry [11-13].

II. Method

The radiation field of interest was of high energy protons with similar energies to those associated with SPE in space applications in the Low Earth Orbit (LEO) environment.

Energy deposition spectra from the incident proton pencil beams were calculated in a cylindrical silicon microdosimeter site, with diameter and height L_{si} equal to 10 μm, set in a water phantom, by means of Geant4 simulations.

The selected experimental set-up allowed to study the tissue-equivalency of silicon, at various depths in the phantom, addressing the issue of the effect of the interactions of primary and secondary particles in the energy deposition spectra, in the microdosimeter site. However it is also important to study the effect of the geometry of the microdosimeter site in the energy deposition spectra, exposing the device to an isotropic radiation field. This issue is of interest for space applications of the SOI technology, and it is addressed in a second paper to be published in the next future, dedicated to the study of the microdosimetric effect of the chord length distribution of different possible shapes of the microdosimeter site.

Water was adopted as the phantom material as a first approximation of the human body. Water is commonly used as a phantom material in dosimetry experiments in addition to other human tissue substitutes such as PMMA [1, 4, and 14]. The silicon tissue-equivalency study in the water phantom represents a reference for further studies considering all the specific human tissues [15].

The energy deposition spectra in the microdosimeter site depend strongly on the LET of the particles traversing the site.

There are two other aspects to consider that can affect the energy deposition spectra in the microdosimeter site; (1) the scattering of protons in the water phantom, and, (2) the secondary particles originated by hadronic interactions.

As a consequence of proton scattering processes within the water phantom it can be expected that many protons will enter the microdosimeter site from directions other than that associated with the direction of the primary beam. The angular distribution of protons approaching the microdosimeter site modifies the path length distribution of the incident protons subsequently affecting the energy deposition spectrum.

The incident proton beam undertakes hadronic interactions in the water phantom and in the silicon microdosimeter site generating secondary particles as protons, neutrons, and recoil nuclei.

The Geant4 simulation was designed to model both the electromagnetic and hadronic physics interactions of all the particles involved in the experimental set-up. The effect of hadronic secondary particles in the energy deposition spectra was considered.

Simulations under the same experimental conditions were repeated with the replacement of silicon as the microdosimeter site material with water.

The methodology to determine the adequacy of the correction factors for the conversion of the microdosimetric spectra between silicon and water involved varying the geometrical size of the water filled microdosimeter site in order to reproduce the microdosimetric spectra obtained in silicon.

The water volume was altered through variation of the microdosimeter site height and diameter, L. A scaling factor, C, was introduced which was given by:

$$C = \frac{L_{Si}}{L},$$

where L_{si} and L indicate the diameter and height of the silicon and water microdosimeter sites respectively.

The result of the study is the factor C^*, corresponding to the best agreement of the energy deposition spectra in the silicon and in the water microdosimeter sites.

For a water cylinder with height h and diameter d, the required scaling is $C^* \cdot h$, $C^* \cdot d$ of silicon.

The energy deposition spectra were calculated in several locations along the Bragg peak curve for monoenergetic 50, 100, 150 and 250 MeV proton beams incident on the water phantom.

The silicon microdosimeter site was positioned at various points along the Bragg curve. The selected positions were representative of the initial plateau (Position I), ascending (Position II), maximum (Position III), and descending (Position IV) zones of the Bragg peak curve. The positions were selected to study the characteristics of the incident proton beam and of its secondary products, at different depths in the phantom. Table I illustrates the depths at which the microdosimeter site was set with respect to the incident proton energy. The maximum incident proton energy was set to 250 MeV, which degrades to approximately 160 MeV traversing 20 cm (Position I) water layer.

A satisfactory value of C^* is that which correctly predicts the scaling between water and silicon at all incident proton energies of interest, at different depths in the water phantom.

TABLE I
DEPTHS AT WHICH THE MICRODOSIMETER SITE WAS SET IN THE WATER PHANTOM, ALONG THE BRAGG PEAK CURVE, WITH RESPECT TO THE INCIDENT PROTON BEAM ENERGY.

Proton Energy (MeV)	Position I	Position II	Position III	Position IV
50	1 cm	2 cm	2.1 cm	2.2 cm
100	4 cm	7.2 cm	7.5 cm	7.7 cm
150	8 cm	15 cm	15.5 cm	15.75 cm
250	20 cm	35 cm	37 cm	38 cm

III. The Geant4 Simulation

A Geant4 application was developed to model electromagnetic and hadronic interactions of an incident proton high energy beam and that of the secondary particle production in a water phantom.

Energy deposition spectra within micron sized volumes of both silicon and water were simulated at different points along the Bragg curve of a proton beam. Figure 1 illustrates the experimental set-up for the simulation.

The microdosimeter site had cylindrical geometry with a height and diameter equal to 10 μm. The cylindrical shape of the sensitive volume was selected to be equivalent to that of the second generation SOI microdosimeters with 3D cylindrical volumes [8]. The axis of the cylinder was aligned with the direction of the beam in the Z axis. The microdosimeter site was placed inside a phantom, at several locations along the central beam axis.

The phantom consisted of a water box. Its longitudinal size along the direction of the primary radiation ensured the complete containment of the Bragg peak curve in the phantom. Its transverse size ensured the full transversal containment of the shower of secondary particles, generated by the incident proton beam.

The material of the microdosimeter site was modelled as either silicon or water to allow the resulting microdosimetric spectra obtained in both materials to be directly compared.

The modeled primary radiation field consisted of a pencil beam of monoenergetic protons. The proton energy was varied from 50 MeV to 250 MeV in order to be representative of the range of energies of the Solar Particle Events proton component flux [17].

The physics list that was selected for the simulations modelled both electromagnetic and hadronic physics interactions.

The Standard Package [18] was selected to model the electromagnetic physics interactions of the particles involved in the experimental set-up.

Geant4 elastic and inelastic hadronic processes were active for all the particles involved in the experimental set-up. The fission and capture processes were also active for neutrons. The Geant4 hadronic Paramaterised Elastic model [9] was activated for protons and the associated secondary particles. The Geant4 Bertini cascade model [19] was active for protons, neutrons and pions. The deuteron, triton and α particle inelastic hadronic scattering was modeled with the Low Energy Parameterized model [9]. The Binary Ion Model [20] was active in the case of other ions.

The threshold of production of secondary particles was set equal to 1 μm within both the microdosimeter site and the water region (see Figure 1) in order to track δ-rays in these geometrical components of the experimental set-up only. The sizes of the water cylindrical region were selected in order to exceed the range of the most energetic secondary electrons produced by the incident proton beam. The production threshold of secondary particles was set equal to 1 mm in the rest of the experimental set-up.

This strategy was adopted to achieve better performance in terms of the limited CPU resources without compromising the accuracy of the dosimetric results deriving from the Geant4 simulation.

The optimization was performed using the Geant4 cuts-per-region functionality [10]. This functionality allows the setting of different thresholds of production of secondary particles in different geometrical components of the simulation.

The output of the simulation consisted of the single event energy deposition spectra deriving from the interactions of both primary and secondary particles within the microdosimeter site.

The simulations were performed with Geant4, release 9.0. Data storage and analysis were performed with ROOT 5.14 [21]. DIANE 1.6.0 [22] was adopted as the job execution control framework for parallel execution of the simulations on a dedicated cluster.

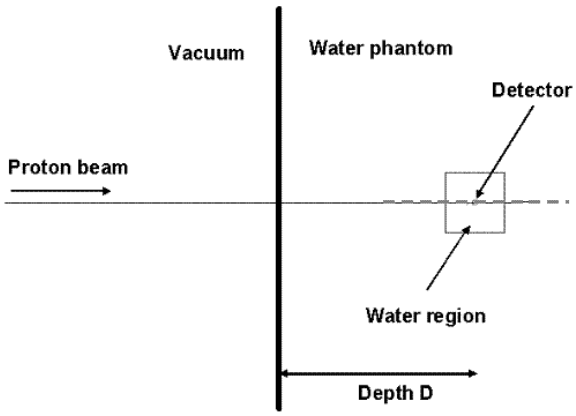

Fig. 1. Experimental set-up of the Geant4 simulation. Monoenergetic protons in a pencil beam were incident perpendicularly to the side of a water phantom. The water phantom was a box. The microdosimeter site was set at a depth *D* along the proton Bragg peak curve. δ-rays were tracked in the water region and in the detector only. The water region was modelled as a cylinder containing the microdosimeter site. The dashed grey line indicates the axis of the cylindrical microdosimeter site and of the cylindrical surrounding water region.

IV. Results

As confirmation of the fact that incident protons approach the microdosimeter site from directions other than that associated with the direction of the primary beam Figure 2 shows the angular frequency of protons entering in the microdosimeter site with respect to the direction of a 50 MeV primary proton beam at depths of 1 and 2.2 cm. At greater depths the angular distribution broadens as scattering of the protons increases.

Figure 3 is a plot of the energy deposition spectra in the silicon microdosimeter site along the Bragg peak curve for the case of a 50 MeV proton beam incident on the water phantom.

As can be observed in Figure 3 at greater depths in the water phantom the energy deposition spectra shift towards

higher energy depositions. This behaviour reflects the fact that protons deposit most of their energy at the end of their range. This is consistent with the mechanism of energy loss of protons in matter.

Taking note of the logarithmic scaling of the data in Figure 3 in the case of shallow depths in the water phantom the energy deposition distribution is relatively sharply peaked. At greater depths the energy deposition distribution becomes broadened as a result of the energy loss straggling and of the multiple Coulomb scattering of the protons.

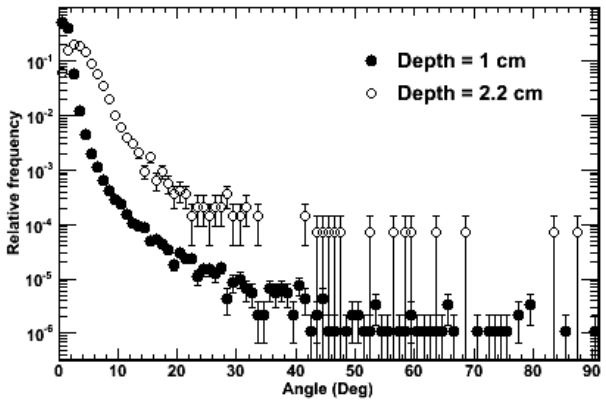

Fig. 2. Angle formed by the direction of incident protons approaching the microdosimeter site and the axis Z corresponding to the direction of protons entering the water phantom. The incident radiation is a 50 MeV proton beam. The microdosimeter site is a water cylinder with diameter and height L=17 μm. The area of the curves is normalized to 1.

The position of the peak of the energy deposition distribution depends mainly on the path length of protons in the microdosimeter site which affects the total energy deposited per event. The position of the peak of the energy deposition spectrum, calculated in the microdosimeter site, shifts towards higher energy deposition values with increasing size L. This behaviour is associated with the increase of the path length of protons in the microdosimeter site.

Preliminary studies performed with a 50 MeV proton beam incident on the water phantom showed that L values with $L <$ 16 μm or $L >$ 19 μm were characterised by a significant shift of the peak of the energy deposition spectrum in the water microdosimeter site with respect to the silicon microdosimeter site. Figure 4 shows the energy deposition spectra in the silicon and water microdosimeter site set at 2 cm depth in the water phantom. The diameter and height L of the water microdosimeter site varied between 10 (corresponding to C =1) and 40 μm (corresponding to C = 0.25).

The preliminary stage of the study allowed the refinement of the range of L values of interest limiting their range to 16 μm < L < 19 μm, corresponding to a respective interval in C of 0.63 to 0.53. The depicted L range (16 μm < L < 19 μm) was selected for further and more detailed investigation to be described in Section V. This methodology allowed an identification of an approximate value of the C conversion factor.

Figures 5-8 show the energy deposition spectra obtained as result of the Geant4 simulation study in both silicon and water volumes (16 μm < L < 19 μm) in the case of a 50 MeV proton beam is incident on the water phantom, along the whole Bragg peak curve.

The low energy depositions (~ O(10 keV)) that can be observed in the plots of Figure 4-8 are mainly due to energy deposition by electrons generated outside the microdosimeter site which scatter into the site.

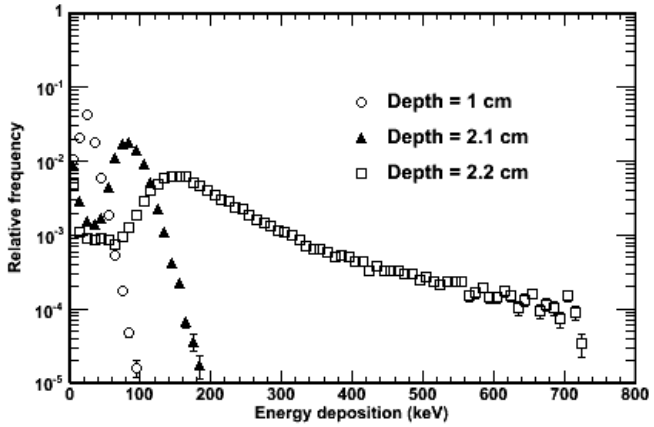

Fig. 3. Energy deposition spectra resulting from a 50 MeV proton beam in the silicon microdosimeter site at different depths in the water phantom. The integral of the curves is normalized to 1.

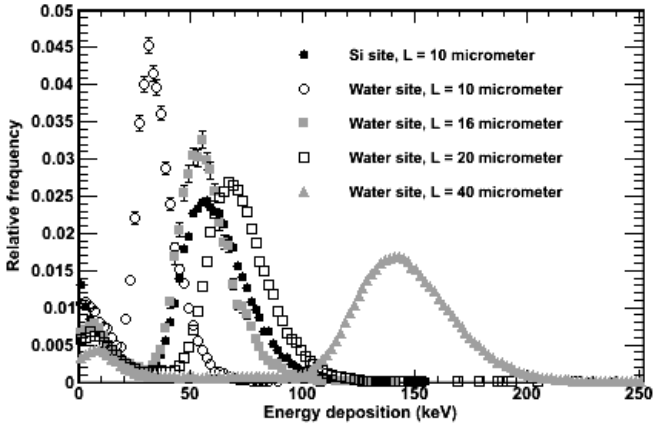

Fig. 4. Energy deposition spectra resulting from a 50 MeV proton beam in the silicon and in water microdosimeter site, at 2 cm depth in the water phantom. The water microdosimeter site has size L equal to 10, 16, 20, 40 μm. The integral of the curves is normalized to 1.

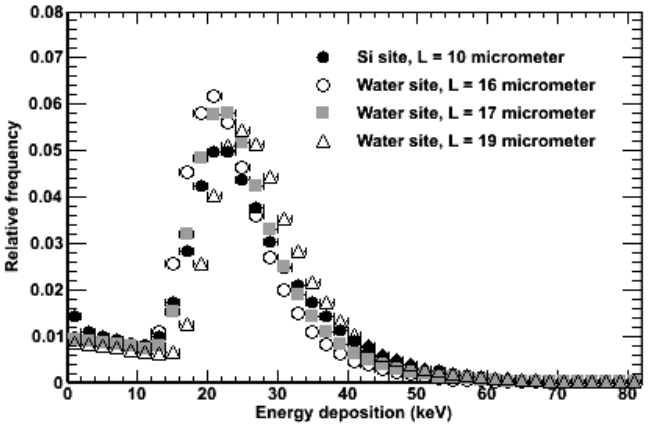

Fig. 5. Energy deposition spectra resulting from a 50 MeV proton beam in silicon and water microdosimeter sites set at 1 cm depth in the water phantom. Depth = 1 cm corresponds to the position in the initial plateau of the Bragg peak curve. The integral of the curves is normalized to 1.

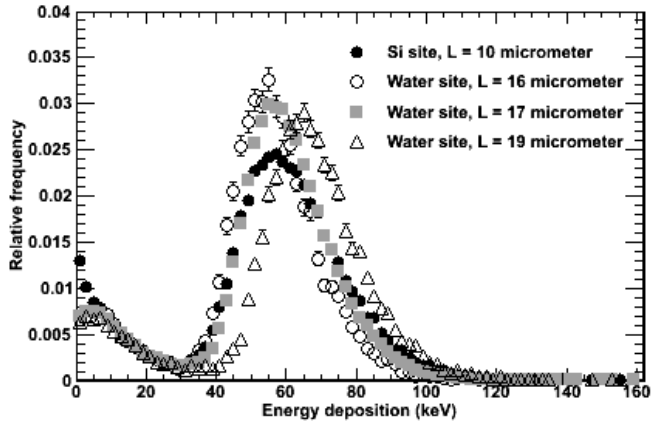

Fig. 6. Energy deposition spectra resulting from a 50 MeV proton beam in silicon and water microdosimeter sites set at 2 cm depth in the water phantom. Depth = 2 cm corresponds to the position in the ascending part of the Bragg peak curve. The integral of the curves is normalized to 1.

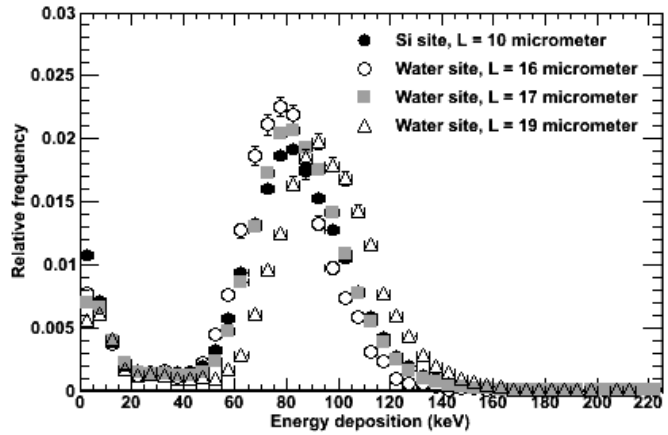

Fig. 7. Energy deposition spectra resulting from a 50 MeV proton beam in silicon and water microdosimeter sites set at 2.1 cm depth in the water phantom. Depth = 2.1 cm corresponds to the Bragg peak position. The integral of the curves is normalized to 1.

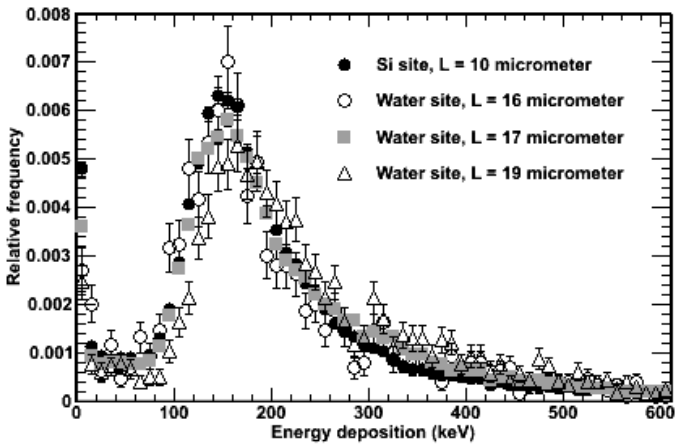

Fig. 8. Energy deposition spectra resulting from a 50 MeV proton beam in silicon and water microdosimeter sites set at 2.2 cm depth in the water phantom. Depth = 2.2 cm corresponds to the position in the descending part of the Bragg peak curve. The integral of the curves is normalized to 1.

V. Statistical Analysis

Quantitative comparisons between the energy deposition spectra in the silicon and in the water microdosimeter sites were performed by means of a Goodness-of-Fit Statistical Toolkit [23, 24], specialized in the comparison of data distributions.

A statistical comparison was executed for each energy of the incident proton beam (50, 100, 150 and 250 MeV), in the positions considered along the Bragg peak curve in the water phantom.

The best agreement between two compared energy deposition distributions corresponded to:

(1) compatible positions of the peak of the energy deposition distribution.

(2) Highest *p*-value, resulting from the statistical comparison of the energy deposition spectra, in the silicon and in the water microdosimeter sites, performed by means of the Kolmogorov-Smirnov test [25, 26].

Phase (1) of the analysis was preliminary to the statistical test of phase (2).

The Kolmogorov-Smirnov test evaluated the compatibility of the energy deposition calculated in the silicon and water microdosimeter sites and its test statistics corresponds to the maximum vertical distance between the two corresponding empirical distribution functions.

The Kolmogorov-Smirnov test was used to compare the left and right branches of the energy deposition distribution separately as well as the full energy deposition spectrum.

The left branch corresponds to the ascending part of the energy deposition distribution culminating with the peak of the curve. The right branch corresponds to the descending part of the energy deposition distribution (refer to Figures 5-8).

The statistical comparison was limited to the energy deposition spectrum with energy depositions greater than 10 keV corresponding to the noise threshold of the SOI silicon device.

The result of the statistical comparison is a *p*-value, representing the test of the null hypothesis that the two

compared energy deposition distributions are compatible. The confidence level $\alpha = 0.05$ was set. A p-value $< \alpha$ would be evidence that the curves are significantly different, and a p-value $> \alpha$ suggests that the curves are not significantly different.

The statistical analysis allowed an objective means of selecting the diameter and height L of the water microdosimeter site to best approximate the energy deposition spectra in the silicon microdosimeter site.

Table II, III, IV, and V report the L of the water microdosimeter site, associated to the best p-values, calculated with the Kolmogorov-Smirnov test.

Of the L values tested between $L = 16$ µm and $L = 19$ µm, a water microdosimeter site with diameter and eight L varying between 17 and 18 µm showed the best statistical agreement in terms of energy deposition distribution with respect to the silicon microdosimeter site, in the case of an incident proton beam with energy ranging from 50 MeV to 150 MeV. $L = 17$ µm and $L = 18$ µm were tested in the case of a 250 MeV proton beam case.

The agreement was observed and maintained in the whole energy range of the incident proton beam (50 MeV $< E <$ 250 MeV), at various depths in the water phantom.

Therefore the C^* value was calculated as:

$$C^* = \frac{C_1 + C_2}{2},$$

where C_1 and C_2 are the C values corresponding to $L = 17$ µm, and $L = 18$ µm, respectively. The result of the study is $C = (0.56 \pm 0.03)$. The error affecting the factor C^* is calculated as the difference between C^* and C_x, where $C_x = C_{1,2}$. The precision of the scaling factor C (~ 5%) is considered satisfactory with respect to other sources of uncertainty, affecting microdosimetric measurements performed with SOI technology and the model of the space radiation environment.

TABLE II
DIAMETER AND HEIGHT L OF THE WATER MICRODOSIMETER SITE, CHARACTERIZED BY THE BEST SILICON –TISSUE EQUIVALENCY. THE ENERGY OF THE INCIDENT PROTON BEAM IS 50 MEV.

	Water microdosimeter site	Left branch p-value	Right branch p-value
Position I	$L = 17$ µm	0.8730	0.9955
Position II	$L = 17$ µm	0.9897	0.8384
Position III	$L = 17$ µm	0.6172	0.9996
Position IV	$L = 17$ µm	0.8580	1.0000

TABLE III
DIAMETER AND HEIGHT L OF THE WATER MICRODOSIMETER SITE, CHARACTERIZED BY THE BEST SILICON –TISSUE EQUIVALENCY. THE ENERGY OF THE INCIDENT PROTON BEAM IS 100 MEV.

	Water microdosimeter site	Left branch p-value	Right branch p-value
Position I	$L = 17$ µm	1.0000	0.5752
Position II	$L = 17$ µm	0.9985	0.9985
Position III	$L = 18$ µm	1.0000	0.9985
Position IV	$L = 18$ µm	1.0000	1.0000

TABLE IV
DIAMETER AND HEIGHT L OF THE WATER MICRODOSIMETER SITE, CHARACTERIZED BY THE BEST SILICON –TISSUE EQUIVALENCY. THE ENERGY OF THE INCIDENT PROTON BEAM IS 150 MEV.

	Water microdosimeter site	Left branch p-value	Right branch p-value
Position I	$L = 18$ µm	1.0000	0.6994
Position II	$L = 18$ µm	1.0000	1.0000
Position III	$L = 18$ µm	0.9730	0.6601
Position IV	$L = 17$ µm	1.0000	1.0000

TABLE V
DIAMETER AND HEIGHT L OF THE WATER MICRODOSIMETER SITE, CHARACTERIZED BY THE BEST SILICON –TISSUE EQUIVALENCY. THE ENERGY OF THE INCIDENT PROTON BEAM IS 250 MEV.

	Water microdosimeter site	Left branch p-value	Right branch p-value
Position I	$L = 18$ µm	0.8730	0.9375
Position II	$L = 18$ µm	1.0000	0.333
Position III	$L = 18$ µm	0.9996	0.3291
Position IV	$L = 18$ µm	0.6994	1.0000

VI. DISCUSSION AND CONCLUSION

In this project a correction method was investigated to convert silicon based microdosimetric measurements to water by means of Geant4 simulations.

The study concerned high energy proton beams that are characteristic of the space SPE proton radiation environment, and of protontherapy.

This work is relevant to radiation protection of astronauts in space with SOI technology currently under consideration as a candidate for a spacecraft monitoring device for future adopt in spacecrafts [3]. The microdosimetric approach measures the radiation effects on the cellular level producing a lineal energy spectrum. When this spectrum is correlated to a well established quality coefficient [27] it is possible to determine the dose equivalent deriving from a mixed radiation field [3]. This work was done in [28], in mixed proton and neutron radiation fields, supporting the possibility of application of SOI microdosimetry in spacecraft crew radiation protection applications.

The project described in this paper determined an adequate methodology to convert microdosimetric measurements performed in silicon to tissue obtained in the presence of a proton radiation field, in an energy range typical of SPE, in the LEO environment. The selected proton energy range can be easily tested in a ground facility at protontherapy centers.

The study utilized a tissue equivalent phantom to approximate the human body with assessments made at different depths in the body. As demonstrated by A. Wroe and co-authors, microdosimetric measurements should be performed at different depths in a phantom to evaluate the harmful biological effects of space radiation in the different tissue components of the human body [3]. The adoption of a phantom embedding the microdosimeter device was also adopted in previous work to study the SOI device performance in the presence of heavy ion radiation field for space applications in [6].

The adoption of a phantom to perform dosimetric calculations for space radiation protection is fully compliant with the guidelines provided by the US National Council on Radiation Protection and Measurements (NCRP) [29] recommending the assessment of biological risk in different tissues of the human body at different depths.

An adequate value of the linear coefficient C^* = (0.56 ± 0.03) was determined to convert microdosimetric spectra from silicon to water for incident proton energies between a few MeV and 250 MeV. The proton low energy limit corresponds to the limit of SOI Technology applicability in proton radiation fields.

For a water cylinder with height h and diameter d, the required scaling is $C^*{\cdot}h$, $C^*{\cdot}d$ of silicon.

The result of the Geant4 simulation study confirms that the ratio value C^* is mainly driven by proton stopping powers in water and in silicon in the case of exposure of the SOI device in a incident proton radiation field with energy E < 250 MeV. Figure 9 shows the Linear Energy Transfer (LET) in water and in silicon multiplied for the factor C equal to 0.56. Agreement within 10% was found over a proton energy range between 3 MeV and 250 MeV. Such agreement may have been predicted in the absence of the water silicon interface which formed part of the simulation based on the ratio of the stopping powers.

The result of this paper confirms the feasibility of the preliminary C^* value, envisaged in previous work by P. Bradley [30]. The former investigation considered a RPP sensitive volume of the SOI device.

The work shown in this paper is a good demonstration that the methodology to convert microdosimetric measurements from silicon to water is valid also for the new cylindrical design of the sensitive volume of the SOI device for high energy protons.

Determining a general methodology to convert silicon microdosimetric spectra to tissue equivalent spectra in any arbitrary mixed radiation field is the next step in this research.

Future studies will investigate the silicon tissue-equivalency in other high LET radiation fields relevant to applications of silicon microdosimetry in radiation protection and in medical physics. In particular the next stage of the project will concern the study of tissue equivalency of silicon in the case of a high energy ion field generating δ-rays with ranges greater than the sizes of the microdosimetric silicon site.

ACKNOWLEDGMENT

The authors would like to thank Alexander Howard for support provided in the domain of Geant4 event biasing as well as Jakub Moscicki and Adrian Muraru for their support in the installation of DIANE.

The authors would like to thank David Boardman for useful discussions.

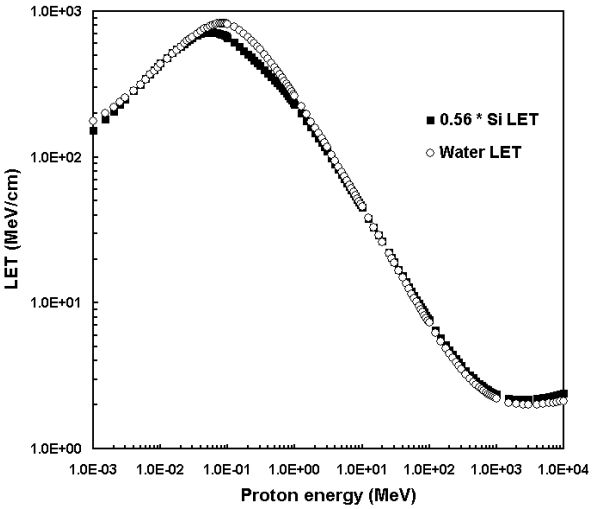

Fig.9. Linear Energy transfer (LET) in water and in silicon. The LET in silicon is multiplied by factor C^* equal to 0.56. LET were calculated from the mass stopping powers, provided in NIST-PSTAR database [31].

REFERENCES

[1] P. D. Bradley, A. B. Rosenfeld, and M. Zaider, "Solid state microdosimetry", *Nucl. Meth. Phys. Res. B*, vol. 184, pp. 135-137, 2001.

[2] International Commission on Radiation Units and Measurements, "Microdosimetry", ICRU Report 36, Bethesda, MD, USA, 1983.

[3] A. J. Wroe, I. M. Cornelius, A. B. Rosenfeld, V. L. Pisacane, J. F. Ziegler, M. E. Nelson, F. Cucinotta, M. Zaider, and J. F. Dicello, “Microdosimetry simulations of solar protons within a spacecraft”, *IEEE Trans. Nucl. Sci.*, vol. 52, no. 6, pp. 2591-2596, 2005.

[4] A. B. Rosenfeld, P. D. Bradley, I. Cornelius, G. I. Kaplan, B. J. Allen, J. B. Flanz, M. Goitein, A. Van Meerbeeck, J. Schubert, J. Bailey, Y. Takada, A. Maruhashi, and Y. Hayakawa, “A new silicon detector for microdosimetry applications in protontherapy”, *IEEE Trans. Nucl. Sci*., vol. 47, no. 4, pp. 1386-1394, 2000.

[5] P. D. Bradley, A. B. Rosenfeld, B. J. Allen, J. Corderre, and J. Capela, “Performance of silicon microdosimetry detectors in boron neutron capture therapy”, *Radiat. Res.*, vol. 151, pp. 235-243, 1999.

[6] A. Wroe, A. Rosenfeld, M. Reinhard, V. Pisacane, J. Ziegler, M. Nelson, F. Cucinotta, M. Zaider, and J. Dicello, “Solid state microdosimetry with heavy ions for space applications”, *IEEE Trans. Nucl. Sci.*, vol. 54, no. 6, 2007.

[7] P. D. Bradley and A. B. Rosenfeld, “Tissue equivalence correction for silicon microdosimetry detectors in boron neutron capture therapy”, *Med. Phys*., vol. 52, no. 11, pp. 2220-2225, 1998.

[8] A. L. Ziebell, W. H. Lim, M. I. Reinhard, I. Cornelius, D. A. Prokopovich, R. Siegele, A. S. Dzurak, and A. B. Rosenfeld, “A novel cylindrical Silicon-on-Insulator microdosimeter for the characterisation of deep space radiation environments”, *IEEE Trans. Nucl. Sci*., *in preparation*.

[9] S. Agostinelli, *et al*., “Geant4 - a simulation toolkit”, *NIM A* , vol. 506, no. 3, pp. 250-303, 2004.

[10] J. Allison, *et al*., “Geant4 Developments and Applications”, *IEEE Trans. Nucl. Sci*., vol. 53, no.1, pp. 270-278, 2006.

[11] A. B. Rosenfeld, A. J. Wroe, I. M. Cornelius, M. Reinhard, and D. Alexiev, “Analysis of inelastic interactions for therapeutic proton beams using Monte Carlo simulation”, *IEEE Trans. Nucl. Sci*, vol. 51, no. 6, pp. 3019-3025, 2004.

[12] A. Rosenfeld, A. Wroe, M. Carolan, and I. Cornelius, “Method of Monte Carlo simulation verification in hadrontherapy with non-tissue equivalent detectors”, *Rad. Prot. Dosim.*, vol. 119, pp. 487-490, 2006.

[13] D. A. Prokopovich, M. I. Reinhard, I. M. Cornelius, and A. B. Rosenfeld, “SOI microdosimetry for mixed field radiation protection”, *Rad. Meas*., vol. 43, pp. 1054-1058, 2008.

[14] A. B. Rosenfeld, P. D. Bradley, I. Cornelius, B. J. Allen, M. Zaider, R. L. Maughan, J. C. Yanch, J. Coderre, J. B. Blanz, and T. Kobayashi, “Solid state microdosimetry in hadrontherapy”, *Rad. Prot. Dos*., vol. 101, pp. 431-434, 2002.

[15] A. Wroe, A. Rosenfeld, I. Cornelius, D. Prokopovich, M. Reinhard, R. Schulte, and V. Bashkirov, “Silicon microdosimetry in heterogeneous materials: simulation and experiment”, *IEEE Trans. Nucl. Sci*., vol. 53, no. 6, 2006.

[16] International Commission on Radiation Units and Measurements, “Tissue substitutes in Radiation Dosimetry and Measurement”, ICRU Report 44, Bethesda, MD, USA, 1989.

[17] A. J. Tylka, J. H. Adams, P. R. Boberg, B. Brownstein, W. F. Dietrich, E. O. Flueckiger, E. L. Petersen, M. A. Shea, D. F. Smart, and E. C. Smith, “CREME96: A Revision of the Cosmic Ray Effects on Micro-Electronics Code”, *IEEE Trans. on Nucl. Sci*., vol. 44, pp. 2150-2160, 1997.

[18] V. N. Ivanchenko, M. Maire, and L. Urban, “Geant4 standard electromagnetic package for HEP applications,” in Proc. Conf. Rec. 2004, IEEE Nuclear Science Symp., Rome, Italy. Paper code: N33-179.

[19] A. Heikkinen, N. Stepanov, and J. P. Wellisch, “Bertini intra-nuclear cascade implementation in Geant4”, in Proc. Computing in High Energy and Nuclear Physics, La Jolla, CA, March 2003, paper MOMT008.

[20] T. Koi, G. Folger, B. Trieu, J. P. Wellisch, I. Cornelius, and P. Truscott, “Ion transport simulation using Geant4 hadronic physics”, in Proc. Computing in High Energy and Nuclear Physics, Interlaken, Switzerland, September 2004, paper 255.

[21] http://root.cern.ch

[22] S. Guatelli, A. Mantero, P. M. Lorenzo, J. Moscicki, and M. G. Pia, “ Geant4 Simulation in a Distributed Computing Environment”, *Nucl. Sci. Symposium Conf. Rec*., vol. 1, pp. 110-113, 2006.

[23] G. A. P. Cirrone, S. Donadio, S. Guatelli, A. Mantero, B. Mascialino, S. Parlati, M. G. Pia, A. Pfeiffer, A. Ribon, and P. Viarengo, “A goodness-of-fit statistical toolkit”, *IEEE Trans. Nucl. Sci.*, vol. 51, no.5 , pp. 2056-2063, 2004.

[24] B. Mascialino, A. Pfeiffer, M. G. Pia, A. Ribon, and P. Viarengo, "New developments of the Goodness-of-Fit Statistical Toolkit", *IEEE Trans. Nucl. Sci.*, vol. 53, no. 6, pp. 3834-3841, 2006.

[25] N.V. Smirnov, “Sur les écarts de la courbe de distribution empirique (Russian/French Summary)”, *Matematiceskii Sbornik N. S*., vol. 6, pp. 3-26, 1939.

[26] N. V. Smirnov, “Table for estimating the goodness-of-fit of empirical distributions”, *Ann. Math. Statist*., vol. 19, pp. 279-281, 1948.

[27] H. H. Rossi and M. Zaider, *Microdosimetry and Its Applications*. Ed. New York: Springer-Verlag, 1996.

[28] A. Wroe, A. Rosenfeld, and R. Schulte, “Out-of-field dose equivalents delivered by proton therapy of prostate cancer”, *Med. Phys*., vol. 34, no. 9, 2007.

[29] NCRP, Report No. 132, “Radiation Protection Guidance for Activities in Low-Earth Orbit”, 2000.

[30] P. Bradley, “The development of a novel silicon microdosimeter for High LET radiation therapy”, PhD Thesis, University of Wollongong, Wollongong, Australia, 2000.

[31] NIST, National Institute of Standards and Technology Composition Database Program, http://physics.nist.gov/cgi-bin/Star/compos.pl?ap